metals

MDPI

Article

Investigations of Fatigue Damage in a Nitriding Low-Carbon Bainitic Steel for High-Performance Crankshaft

Alessandro Giorgetti [1,2,*], Ulisse Millefanti [2], Vincenzo La Battaglia [1] and Paolo Citti [2]

[1] Department of Industrial, Electronic and Mechanical Engineering, Roma Tre University, 00146 Rome, Italy
[2] Department of Engineering Science, Guglielmo Marconi University, 00193 Rome, Italy
* Correspondence: alessandro.giorgetti@uniroma3.it

Abstract: In the automotive environment, the need to increase the performance of materials requires extra engineering efforts. The possibility of developing new materials is strategically important. Indeed, alternative solutions in terms of material choice allow designers to optimise their projects and keep competitive production costs. Traditional quenched and tempered steels are usually used for highly stressed components, and possible alternatives could be important competitive opportunities. One possible substitute is using bainitic steels to exploit their economic advantages while maintaining acceptable mechanical performances. This paper explores the fatigue life behaviour of a new low-carbon bainitic steel for applications requiring case hardening treatment obtained by the nitriding process. A high-cycle fatigue (HCF) strength assessment is conducted through a test campaign to compare treated and untreated material. The improvement in fatigue strength is evaluated as well as the study of fracture surfaces, residual stress, and microhardness profiles to assess in detail the effectiveness of the nitriding process. It is found that the nitriding leads to an improvement in fatigue life but not as much as expected because of the low ductile behaviour of this steel, the high speed of stress application added, and the embrittlement of the nitriding treatment, as confirmed through fracture surface analysis.

Keywords: mechanical component; material selection; microstructure; fatigue life estimation; bainite; HCF; SEM analysis; EDS analysis; residual stress analysis

Citation: Giorgetti, A.; Millefanti, U.; La Battaglia, V.; Citti, P. Investigations of Fatigue Damage in a Nitriding Low-Carbon Bainitic Steel for High-Performance Crankshaft. *Metals* **2022**, *12*, 2052. https://doi.org/10.3390/met12122052

Academic Editors: Delphine Retraint and Zhidan Sun

Received: 31 October 2022
Accepted: 26 November 2022
Published: 29 November 2022

1. Introduction

Bainitic grade steels are utilised in several industrial applications and automotive powertrain components. Advantages characterise this kind of steel in terms of process time and overall costs compared with tempered and quenched steels. In fact, bainitic grade steel permits high mechanical properties without the time and economic burden of performing numerous heat treatments, such as in tempered and quenched steels. Evaluating the high-cycle fatigue (HCF) performance of martensitic grade steel is crucial for correctly assessing whether such materials should be used in specific high-value-added applications competing against high-strength steel. This information could be used in the materials selection phase [1–3] and to identify a better solution in many industrial applications [4]. This is particularly true in contexts where the materials are highly stressed, and the loads are time-dependent. An example of this type of component is the crankshaft for an internal combustion engine.

So dealing with fatigue in highly stressed components, it is interesting, as discussed in the paper by Citti et al. [5], to evaluate the fatigue limit of typical bainitic steel considering not only the untreated material but also the nitriding as a case hardening treatment. The nitriding process allows the development of high fatigue performances necessary for highly stressed mechanical components. Indeed, nitriding treatment for traditional steels allows adding 50% or more to fatigue resistance to the untreated material, as shown by several authors [6–10]. This increase in the fatigue limit is due to compressive residual stresses on

the nitrogen diffusion layer below the actual applied stress onto the component itself. This article aims to study a bainitic steel's behaviour after a traditional gas nitriding process in terms of nitrogen diffusion and fatigue limit increase compared to the untreated material. The method for the investigation of HCF behaviour is rotating bending. The samples were designed and manufactured in line with the machining usually used for crankshafts.

The following paragraphs show:

- Section 2, Materials and Methods, describes the Characterization of the steel in terms of chemical composition, static mechanical properties, heat treatments cycle process, and description of the specimens used for the HCF tests carried out;
- Section 3, Results and Discussion, shows microstructure analysis of nitrided and untreated specimens, the results in terms of the HCF performance of the material, the fracture surface analysis, and the residual stress analysis;
- Section 4, the Conclusion, summarises the results, focusing on the limitations and future developments.

2. Materials and Methods

Low-carbon bainitic steel has been studied in this paper. Table 1 shows the chemical composition of the analysed steel obtained using an Arun Artus 8 spectrometer (ARUN Technology Limited, Crawley, UK). The steel is received in vacuum air-remelted bars 80 mm in diameter after a pseudo-forging treatment at 1000 °C for 45 min and air cooling to room temperature (cooling rate range 0.1–0.2 °K/s, room temperature 20 °C). Smaller squared raw bars are cut out from the main bars at an equal distance from the centre. Finally, a stress relief heat treatment at 550 °C for 8 h is carried out. From this condition, specimens are machined, and the nitriding heat treatment in a static gas oven for 72 h at 515 °C is carried out too.

Table 1. Chemical composition of the steel used in this study (wt.%).

Composition	wt%
C	0.16
Mn	1.48
Si	0.97
Cr	1.43
S	0.05
Ni	0.18
Mo	0.14
Cu	0.23
Others	0.17 V
Fe	Bal.

In Figure 1, the heat treatment cycle is summarised, also considering the nitriding phase.

The material's static mechanical properties (ISO 6892-1) at the core after the heat treatment cycles are collected in Table 2. The machine utilised for the tensile test is a Galdabini Quasar 200 (Galdabini, Cardano al Campo, Italy) equipped with an extensometer in strain control.

Table 2. Mechanical characteristics of steel after heat treatments cycle.

Characteristic	Value
Proof strength Rp0.2 [MPa]	952
Tensile strength Rm [MPa]	1124
Percentage elongation	18

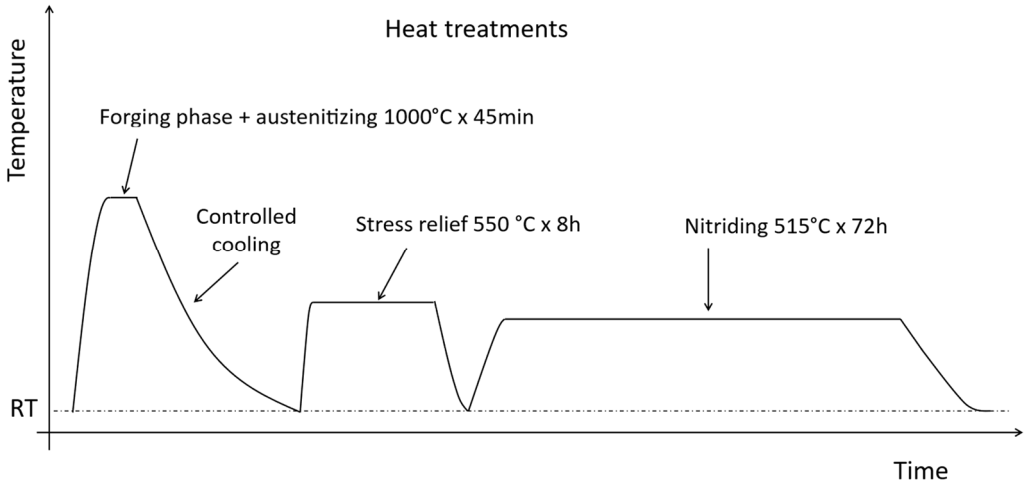

Figure 1. Scheme of the heat treatment cycle performed on the specimens (RT—Room Temperature, 20 °C).

The specimens for the rotating bending fatigue are realised following similar machining phases for an engine crankshaft. For the nitrided specimens, the resistant section is firstly ground and then nitrided. A final grinding (0.05 mm material removal) plus polishing is carried out at the end of the nitriding heat treatment. Identical machining operations are also performed for the non-nitrided specimens (untreated specimens). The final surface roughness values achieved on specimens are comparable with the surface roughness values of a typical crankpin using a Taylor Hobson surface roughness tester (Taylor Hobson, Leicester, UK). Figure 2 shows the characteristics of the finished specimen before the bending test. Table 3 shows the average and standard deviation of the final roughness parameters measured on the specimens after final polishing.

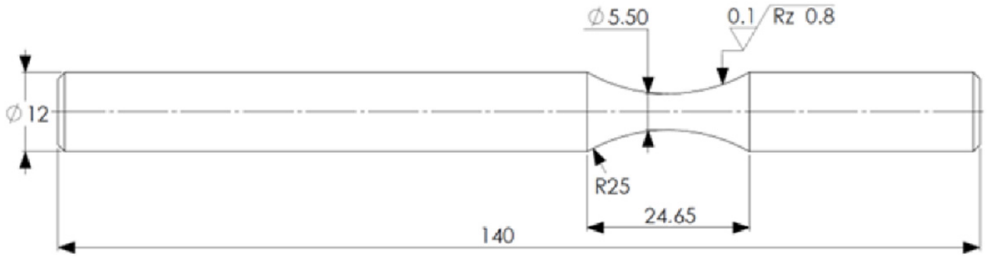

Figure 2. Technical drawing of the finished ground and polished specimen.

Table 3. Roughness parameters measured on the calibrated zone of samples.

Characteristic	Ra [μm]	Rz [μm]	Std. dev. Ra	Std. dev. Rz
Untreated specimens	0.09	0.76	0.016	0.174
Nitrided specimens	0.10	0.79	0.021	0.206

Each specimen is cleaned and degreased in heptane solvent before the tests.

For the evaluation of the nitriding process, hardness profile curves on specimens are carried out. The nitriding depth profiles are realised by interpolating micro Vickers hardness indentations by 0.5 kg load for 15 s using an FM-7 microhardness tester (Future Tech, Tokyo, Japan).

Rotating fatigue tests are performed on a single-point bending test machine at a frequency of 50 Hz in air. Figure 3 shows the machine's scheme and the specimen's clamping system.

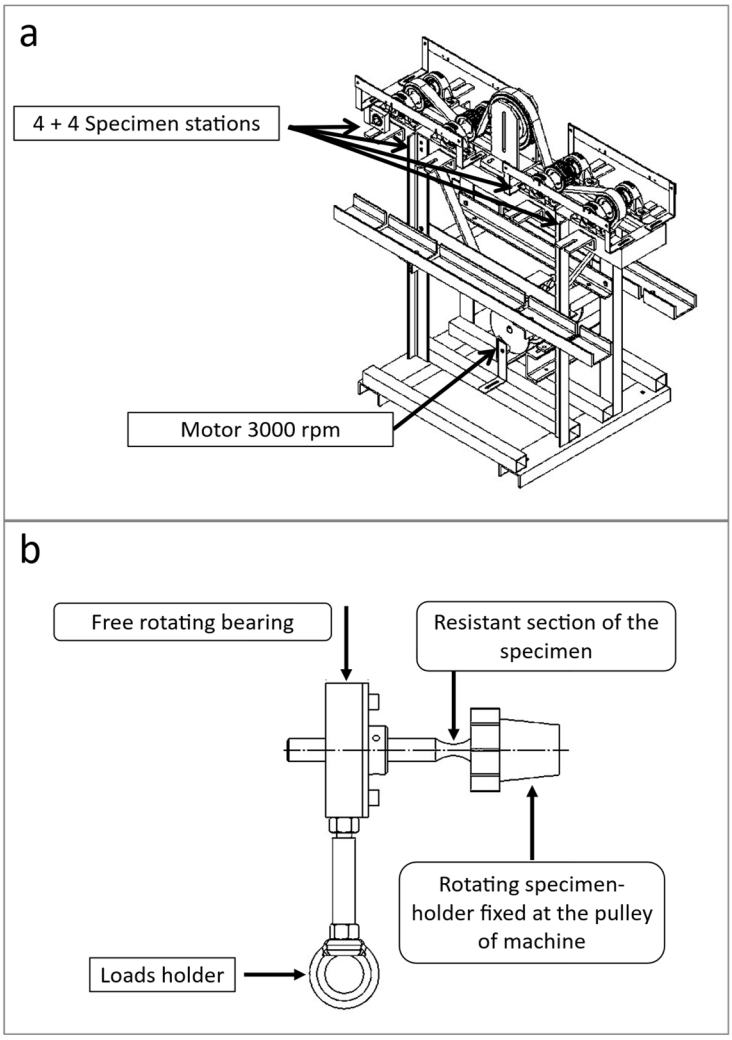

Figure 3. (**a**) Scheme of the eight stations rotating fatigue machine; (**b**) clamping system for the specimen.

The staircase method (for more detail on the calculation, see [11,12]) is used to identify the fatigue limit at 10^7 cycles at the constant step of load variation (25 MPa). There is no observation of heating effects on the specimens during fatigue testing, and pure rotating bending conditions are correctly maintained.

The fracture surfaces of the specimens are examined under stereoscopic using Olympus BX51M (Olympus soft imaging solutions GmbH, Münster, Germany). The morphology of the fractures is analysed by Scanning Electron Microscope (SEM) Zeiss Sigma 300 VP (Zeiss, Oberkochen, Germany, 15 KeV, 2.25 A) to evaluate the crack nucleation and fatigue development. The residual stress analysis is made using an Xstress G3 diffractometer (Stresstech, Jyväskylä, Finland) collimator with a diameter of 2 mm based on the d vs. $\sin^2 \Psi$ method.

3. Results and Discussion

3.1. Microstructure Analysis

Metallographic cross-sections are performed both for the nitrided and the untreated specimens. The microstructure of the material is analysed after etching by Nital 2%. Figure 4a,b show such microstructures at the core and nearby external surfaces of a nitrided specimen without the final grinding and polishing phase. Figure 4c shows the compound layer developed in this steel. The average thickness of this layer is about 13 µm. Some nitriding lamellae developing from the compound layer are detected, and a not-closed

net is formed at grain boundaries. Figure 4d shows the microstructure of the untreated specimen, which appears identical to the nitrided specimen microstructure at the core.

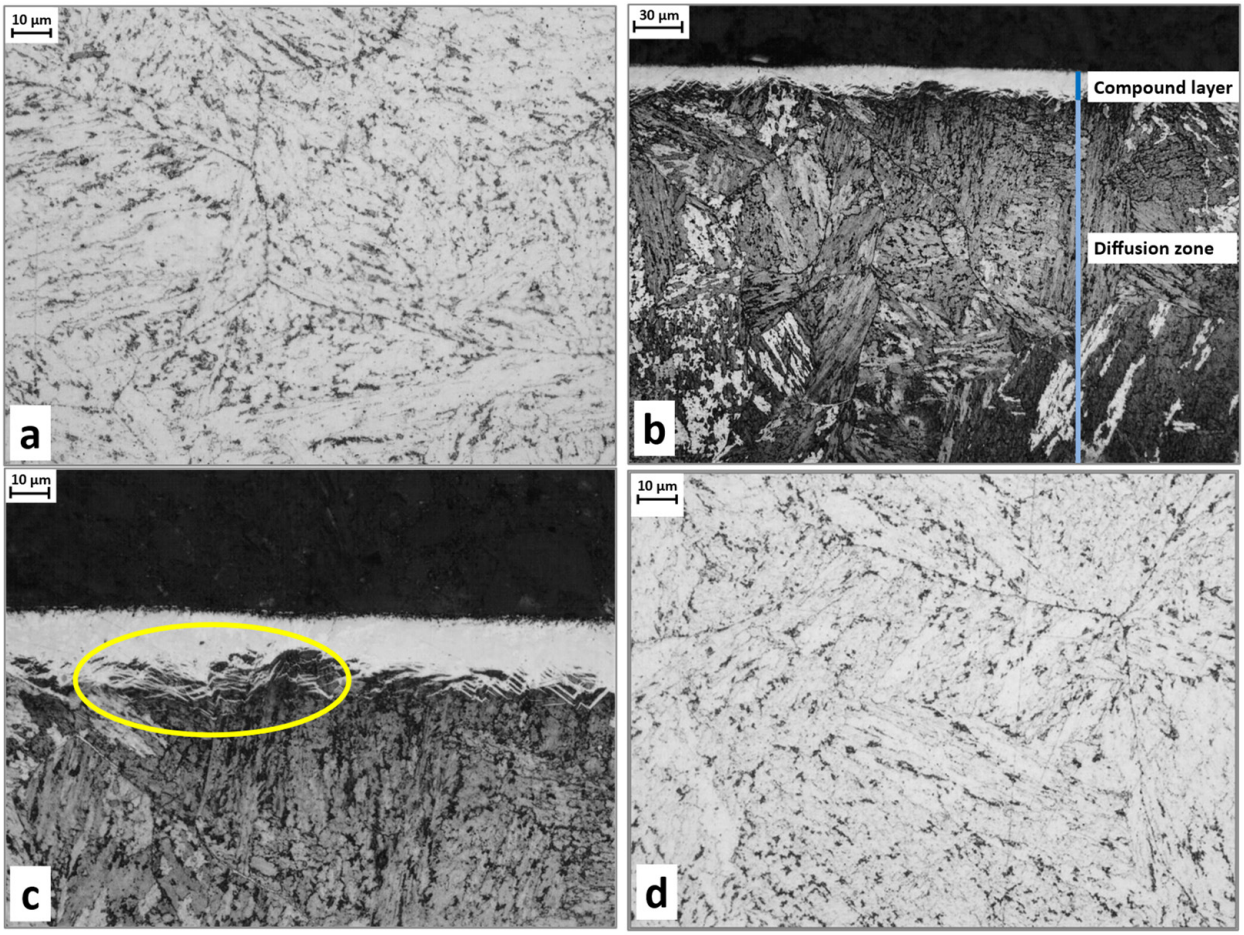

Figure 4. Microstructure analysis: (**a**) core microstructure example of nitrided and untreated specimen 500×; (**b**) compound layer and diffusion zone 200×; (**c**) compound layer detail with nitriding lamellae generated 500× after Nital 2% etching; (**d**) core microstructure of the untreated material specimen 500× after Nital 2% etching.

As known, the gas nitriding process generally performed between 500–580 °C generates a compound layer, also called the "white layer", of intermetallic compounds (nitrides and carbonitrides: γ_Fe_4N phase or ε_-Fe_2N phase) [13,14]. This layer is very brittle, and its debris could potentially interpose between mechanical components such as crank pins and bearings, generating failure. So in such applications, it is removed.

Typically, the nitrogen diffuses in this steel, generating a modified structure or "diffusion zone" for a depth of 0.1–0.5 mm. This region consists of stable nitrides generated by the thermochemical reaction of nitrogen with steel.

The main advantage in terms of fatigue resistance, in particular in bending stressed applications, given by the nitriding process consists of generating a compressive state below the surface because of the diffusion of nitrogen and the lattice deformation.

Figure 5 shows two curves of the nitriding depth profiles of the specimens. Two transversal sections by specimen are analysed. The first is in the ground and polished section, and the second is in a raw part without final grinding and polishing operations. The standard deviations of the measurements by every indentation are also added to the graph. The two curves show a constant shift of about 0,05 mm due to the final grinding and polishing.

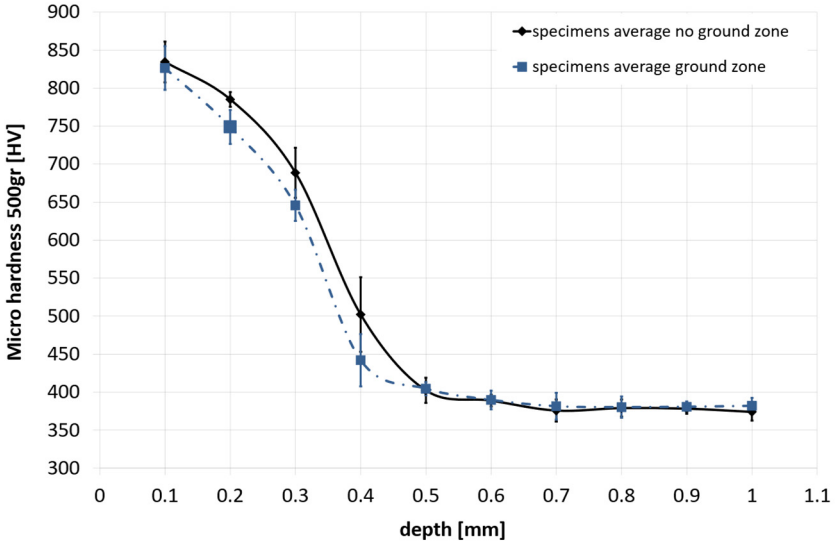

Figure 5. Nitriding depth curves for the ground and polished section (black line) and the not-final ground section (blue dashed line).

Four reference depths of the nitriding case have been evaluated regarding the nitriding heat treatment. They are set at 525 Vickers, core plus 100 Vickers, core plus 50 Vickers, and core plus 10% core hardness Vickers. Table 4 reports the core hardness and depth values at the various reference points. The nitriding depth measured could be compared with traditional nitrided quenched and tempered steels [15].

Table 4. Core hardness and nitriding depth measurements at various references.

Headings	Not Ground Zone	Ground and Polished Zone
Core HV	375	375
Depth 525 HV	0.41 mm	0.36 mm
Depth core + 100 HV	0.43 mm	0.39 mm
Depth core + 50 HV	0.48 mm	0.43 mm
Depth core + 10% hardness HV	0.50 mm	0.46 mm

3.2. HCF

The staircase method is carried out using 20 specimens to evaluate the fatigue limit. In detail, the limits at the 10th, 50th, and 90th percentile of survival are computed. Table 5 shows the limits obtained through the staircase method.

Table 5. Fatigue limits reached by untreated specimens after staircase fatigue test.

Heading	10th of Survival	50th of Survival	90th of Survival
Fatigue limit [MPa]	652	626	601

Figure 6 shows the complete staircase with each single test result. The white circles represent runout cases (number of cycles > 10^7 cycles), while the black circles represent the failure cases. Table 6 details the number of failure cycles and the bending stress values applied for each specimen. Notice that the maximum number of cycles counted with a failure of the specimen is 3.4×10^6; above, only runouts of the specimens are collected, enhancing the knee for the S/N curve of the steel. The ratio of the Rm value with the fatigue limit at the 50th percentile is above 50% (56%). This value is in line with high-performance quenched and tempered steel families reported by several studies [16,17].

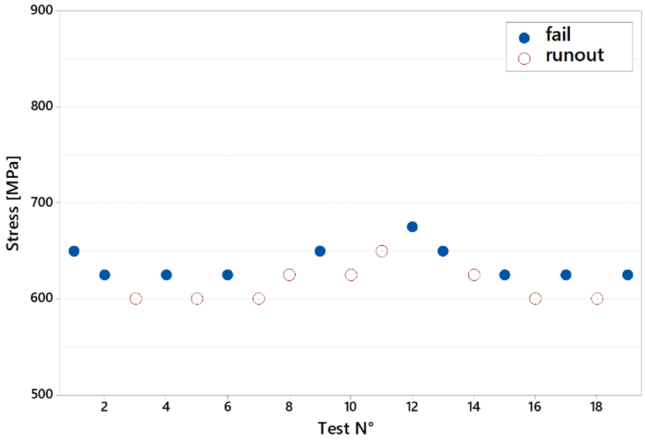

Figure 6. Complete staircase results of untreated specimens.

Table 6. Stress and cycles by each test of the staircase of the untreated specimens.

Test n°	Stress [MPa]	Cycles
1	650	6.079×10^5
2	625	4.367×10^5
3	600	runout
4	625	2.358×10^6
5	600	Runout
6	625	2.972×10^6
7	600	runout
8	625	runout
9	650	1.381×10^5
10	625	runout
11	650	runout
12	675	3.619×10^5
13	650	3.430×10^6
14	625	runout
15	650	5.690×10^5
16	625	3.692×10^5
17	600	runout
18	625	5.238×10^5
19	600	runout
20	625	9.911×10^5

About the staircase performed onto the nitrided specimens, the fatigue limit at 10^7 cycles for the 50th percentile survival is at 706 MPa, while for the 10th and 90th percentiles, the values are 723 MPa and 690 MPa, respectively (Table 7). The increase in the fatigue limit is about 13%. This value is relatively low if compared with other quenched and tempered steels after the nitriding heat treatment, which can increase their fatigue limit much more compared with untreated conditions [18–20]. It is also possible to notice a certain level of data scattering in the presence of fatigue life below 2×10^7 cycles, as suggested by Gui et al. [21].

Table 7. Fatigue limits reached by nitrided specimens after staircase fatigue test.

Heading	10th of Survival	50th of Survival	90th of Survival
Fatigue limit [MPa]	723	706	690

Figure 7 shows the results of each nitrided specimen tested. Table 8 details the number of cycles before the specimen fails in the various tests performed.

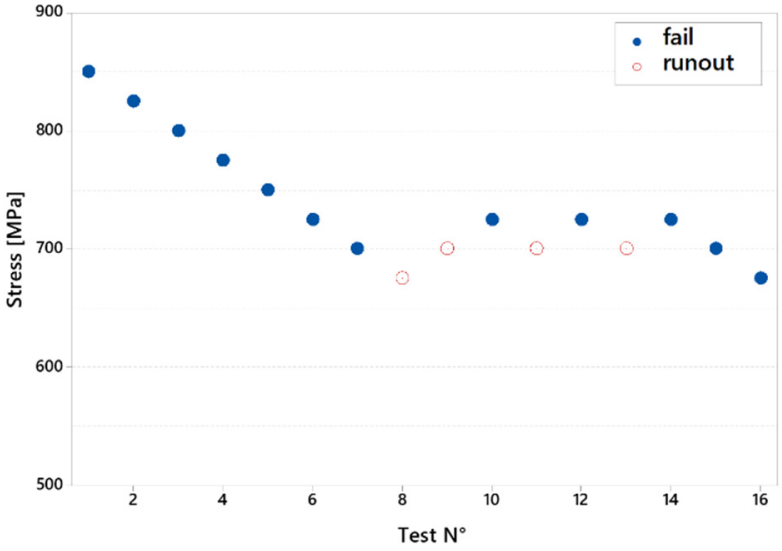

Figure 7. Complete staircase results of nitrided specimens.

Table 8. Stress and cycles by each test of the staircase of the nitrided specimens.

Test n°	Stress [MPa]	Cycles
1	850	1.805×10^6
2	825	1.780×10^6
3	800	1.397×10^6
4	775	3.995×10^6
5	750	6.865×10^6
6	725	3.053×10^6
7	700	7.369×10^6
8	675	runout
9	700	runout
10	725	2.316×10^6
11	700	runout
12	725	5.668×10^6
13	700	runout
14	725	1.793×10^6
15	700	7.310×10^6
16	675	5.359×10^6

Notice in Figure 8 that in several cases, the number of cycles measured at the failure of the specimens is between 4×10^6 and 10^7 cycles, while no more than 3.4×10^6 cycles with failure are detected for the untreated specimens. Therefore, the knee of the S/N curve for the nitrided specimens is shifted at a higher number of cycles than the untreated steel one. This phenomenon of later initiation of fatigue cracks could be due to nitriding, as suggested by Terent'ev et al. [19].

3.3. Fracture Surface Analysis

The untreated specimens follow typical fatigue development from external surface nucleation to the core. Nucleation in these test specimens occurs from the outer surface and without the presence of any inclusions, as evidenced by specific EDS analysis. In Figure 9a, taken from the stereoscopic instrument, it is possible to assess the development of the fatigue and the final fracture of a specimen. About 30% of the resistant section fails by fatigue propagation. Figure 9b shows a band of crash-fractured material with brittle morphology identical to the crash-fractured heart zone in the transition zone between the fatigue propagation zone and the crash-fractured zone. (detailed in Figure 9c). This phenomenon always occurs near the separation of fatigue and crash propagation.

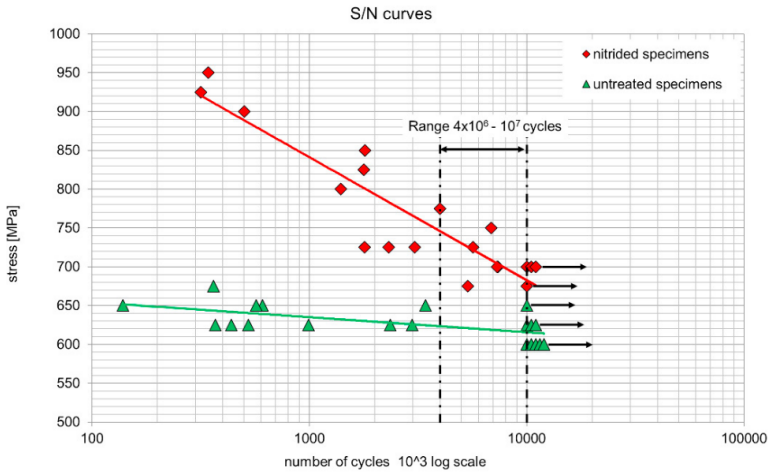

Figure 8. S/N curve of untreated and nitrided specimens.

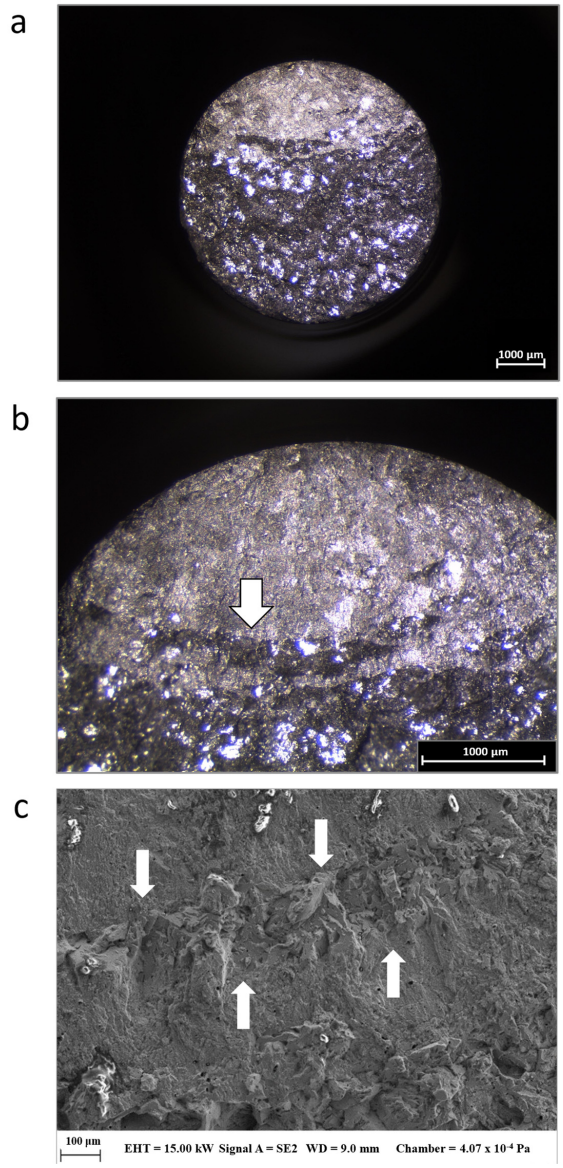

Figure 9. Surface fracture analysis: (**a**) example of final fracture surface for the untreated specimen, stereoscopic image 10×; (**b**) 25×; (**c**) detail of the morphology of the broken crash area within the fatigue propagation zone (identified by the white arrow in (**b**)).

Moreover, Table 9 reported the fatigue propagation values for all the broken specimens.

Table 9. Stress and fatigue propagation by each test of the staircase of the nitrided specimens.

Test n°	Stress [MPa]	Fatigue Propagation [mm]
1	650	1.886
2	625	1.887
4	625	1.794
6	625	1.872
9	650	2.010
13	650	1.982
15	650	1.888
16	625	1.714
18	625	1.705
20	625	2.262
13	650	1.982
15	650	1.888
16	625	1.714

The morphology of the sudden fracture at the SEM reveals a brittle behaviour of the material with quasi-cleavage fracture (Figure 10a) that contrasts with the tensile test performed (Figure 10b). Indeed, specimens showed high elongations and ductility at the fracture surface with dimples (some brittle cracks are detected at grain boundaries). The different speeds of solicitations could justify the different behaviour. In other words, solicitations at high speed, such as the bending fatigue test carried out in this study, can completely change the behaviour of the steel passing from a ductile to a brittle one.

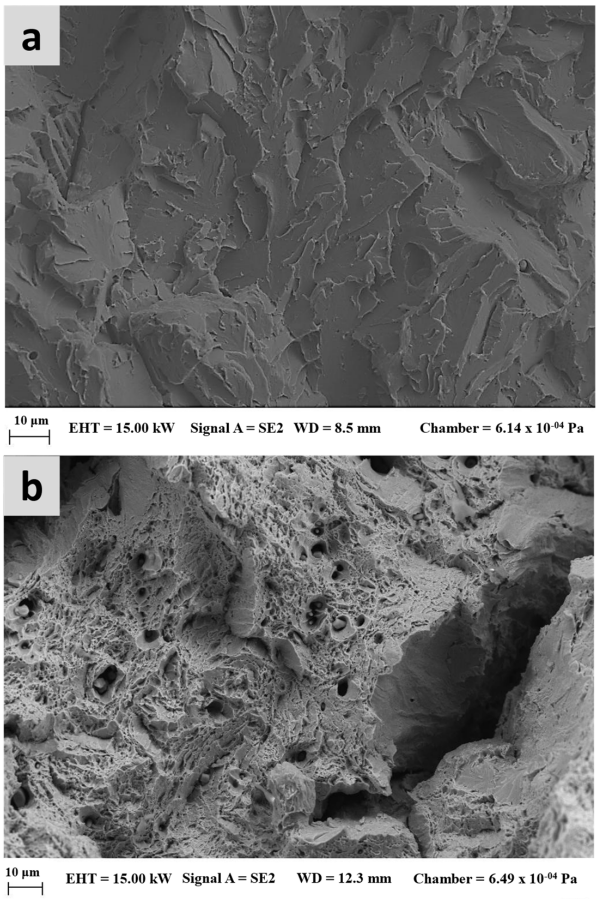

Figure 10. (**a**) Brittle fracture at the core of the untreated specimen. (**b**) Ductile fracture of the tensile specimen with few brittle zones.

About nitrided specimens, subsurface nucleation is detected. Figure 11 shows examples of the fracture analysed by stereoscopic instrument (Figure 11a,b) and with SEM (Figure 11c,d), with the typical fish-eye fatigue propagation [7,22]. In all tests, the fish-eye area appears circular and white, with the crack nucleation site as a dark area in the centre. This dark area is known as the "Optically Dark Area" (ODA) by Murakami et al. [23] or as the "fine granular area" (FGA) by Sakai et al. [24] and "Granular-Bright-Facet" (GBF) by Shiozawa et al. [25]. Notice that the fatigue propagation is limited to a small portion of the resistant section, about 16%.

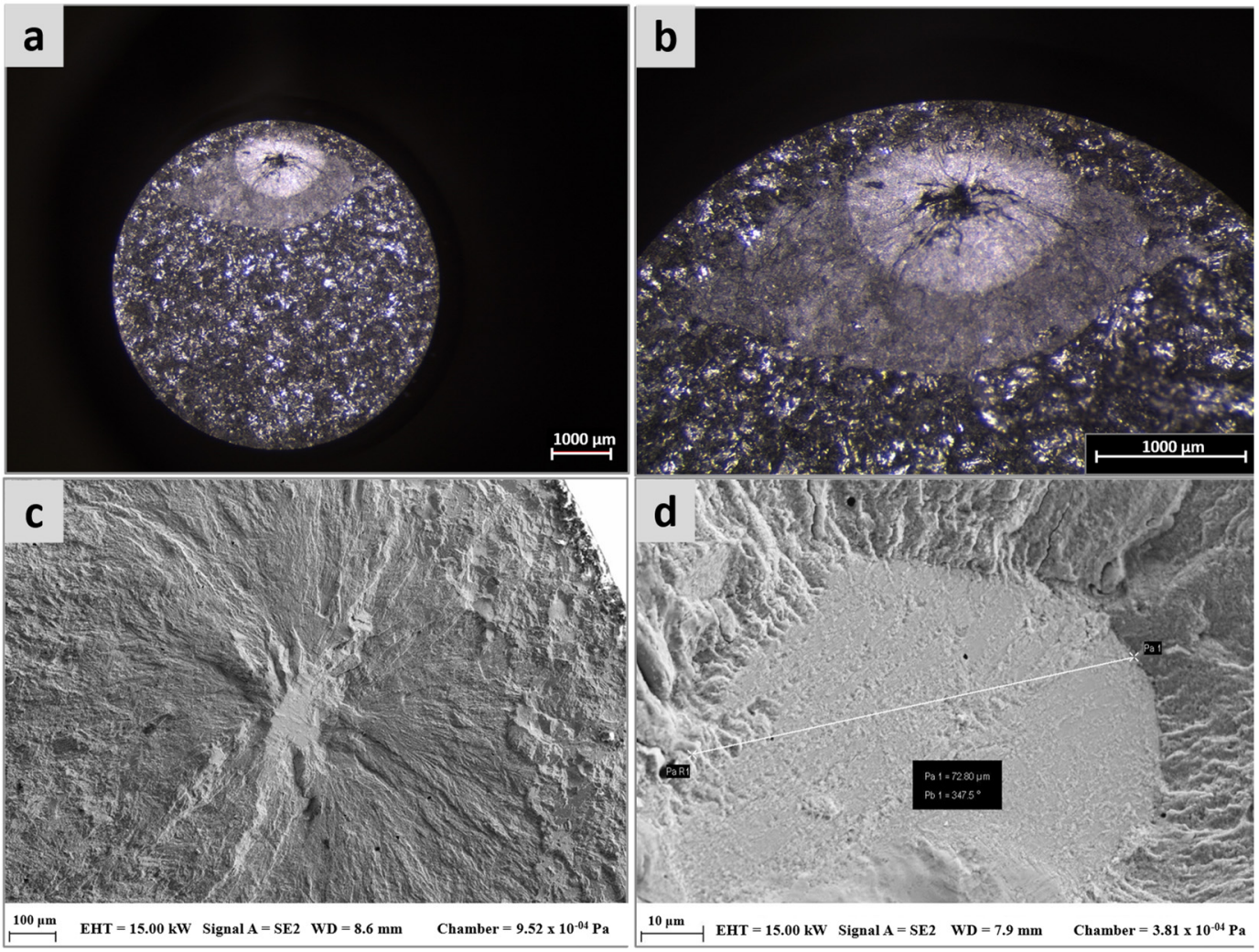

Figure 11. (**a**) example of the final fracture surface of the nitrided material specimen; 10× stereoscopic image. (**b**) Example of subsurface fatigue propagation of nitrided material specimen; note fish-eye nucleation with ODA; 25× stereoscopic image. (**c**) Fish-eye nucleation example. (**d**) Matrix failure detail.

Matrix nucleation and fatigue propagation, observed by the SEM analysis (Figure 11c,d), are similar to the phenomena defined as supergrain nucleation by Zhou et al. [17] and Huang et al. [22]. Differently from some other authors' studies as Zhang et al. [26], Murakami et al. [27], and Bell et al. [15], the nucleation cause cannot be associated with inclusion in the specimens analysed. A confirmation of this is obtained through the EDS analysis of the fish-eye nucleation zone, which did not detect any traces of elements not common to steel (Figure 12).

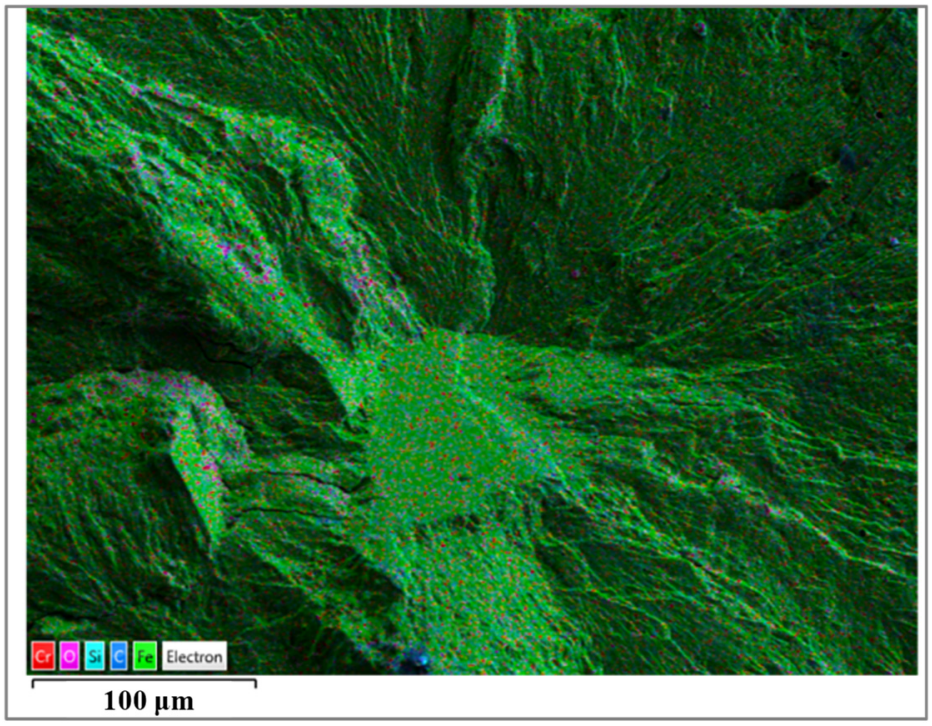

Figure 12. EDS analysis of the fish-eye nucleation zone.

The nucleation depths from the external surface have been measured by SEM in each broken specimen. These values are used to compute the equivalent applied stresses at the nucleation point by stress distribution of bending along the cross sections of specimens. Table 10 reports the values of these depths measured by each test and the computed values of stresses acting on the nucleation points.

Table 10. Fatigue nucleation depth and equivalent stress evaluated at the nucleating point.

Test n°	Fatigue Nucleation Depth [mm]	Equivalent Stress at the Nucleation [MPa]
1	0.748	618
2	0.532	664
3	0.492	656
4	0.709	574
5	0.574	593
6	0.457	604
7	0.533	564
10	0.580	571
12	0.650	553
14	0.780	519
15	0.544	561
16	0.647	516

First of all, must be highlighted the fact that the nucleation depths measured are just above the case/core material transition, where the compressive stresses convert to tensile stresses [7,17]. Secondly, the average of the equivalent stresses is 583 MPa, close to the fatigue limit measured by the staircase test for untreated specimens. This justifies the matrix breakage at the subsurface for all specimens.

The SEM analysis for the nitrided specimens reveals a brittle behaviour at the core of the material (Figure 13a), as seen on the untreated specimens. Moreover, a transgranular fracture for the nitriding zone with no fatigue propagation onto the nitriding case is detected nearby and far away from the nucleation point (Figure 13b,c).

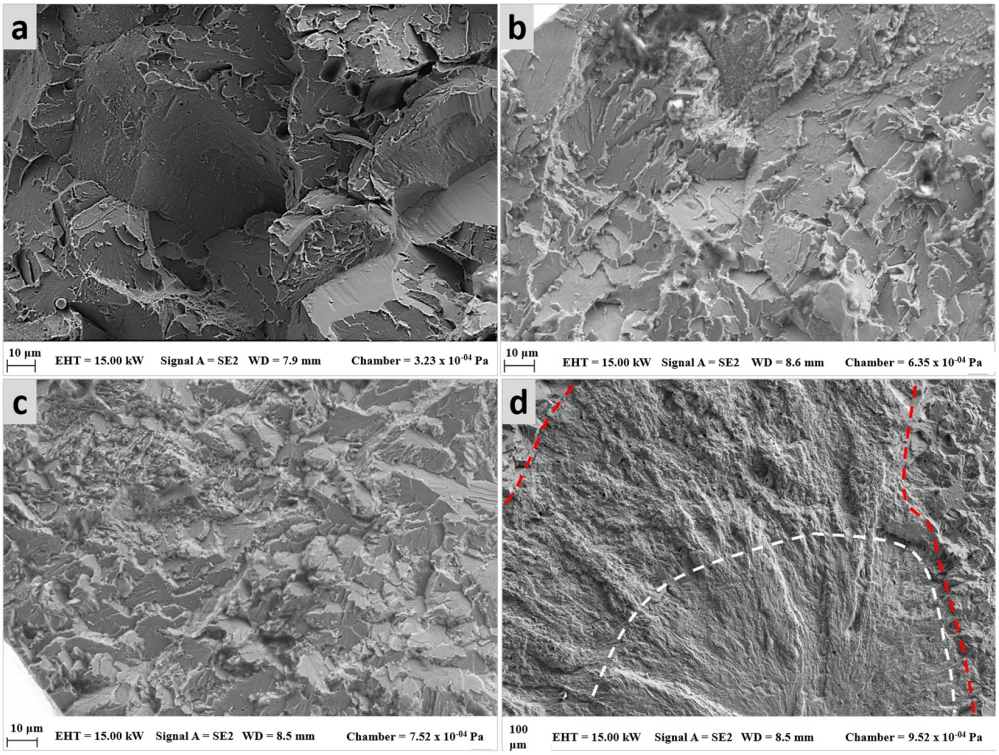

Figure 13. (**a**) Brittle fracture at the core of the material; (**b**) nitriding case nearby final failure with brittle fracture; (**c**) nitriding nearby fatigue nucleation with brittle transgranular fracture; (**d**) fatigue propagation in the fish-eye zone (white line) and crash breaks in the heart zone (red left margin) and nitrided zone (red right margin).

With regard to the crack advance zone, no morphological differences are found with what is seen in the non-nitrided specimens. A detail of the crack advance is shown in Figure 13d. It is possible to note the fish-eye zone at the bottom delimited by the white dashed line at the top the fatigue propagation with similar morphology to that already seen in the non-nitrided samples, and at the left and right limits of the image, the zones characterised by the crash fracture in the core and the nitrided layer, respectively (red lines).

The so brittle behaviour of the bainitic material obtained by the tests justifies that fatigue propagation is limited. Indeed, no plasticity is allowed, so the initial crack as nucleates determines a rapid fatigue development.

The sizes of the fish-eye zones have been evaluated for the nitriding tested specimens. Table 11 shows these values obtained.

Table 11. Fish-eye area evaluation.

Test n°	Fish-Eye Area [mm^2]
1	0.65
2	0.87
3	0.74
4	0.84
5	1.16
6	1.35
7	1.42
8	1.40
9	1.47
10	1.69

Using data in Table 11, it is possible to evaluate the correlation between the fish-eye area, the number of cycles (Figure 14), and the test loads (Figure 15).

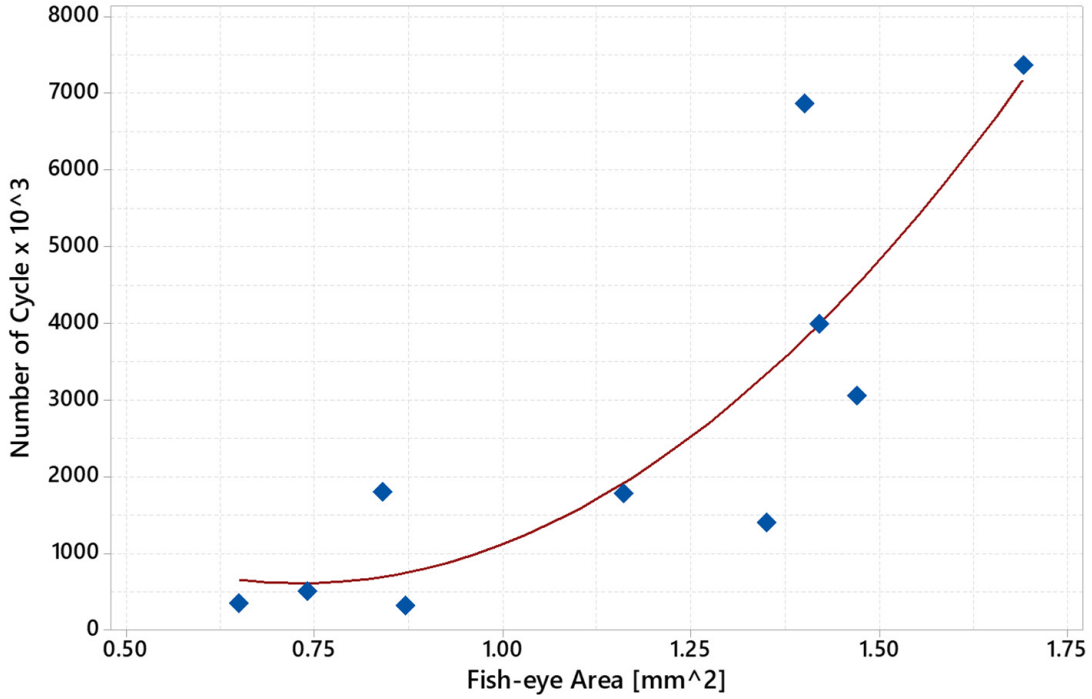

Figure 14. Scatter Plot of the correlation between fish-eye area and number of cycles.

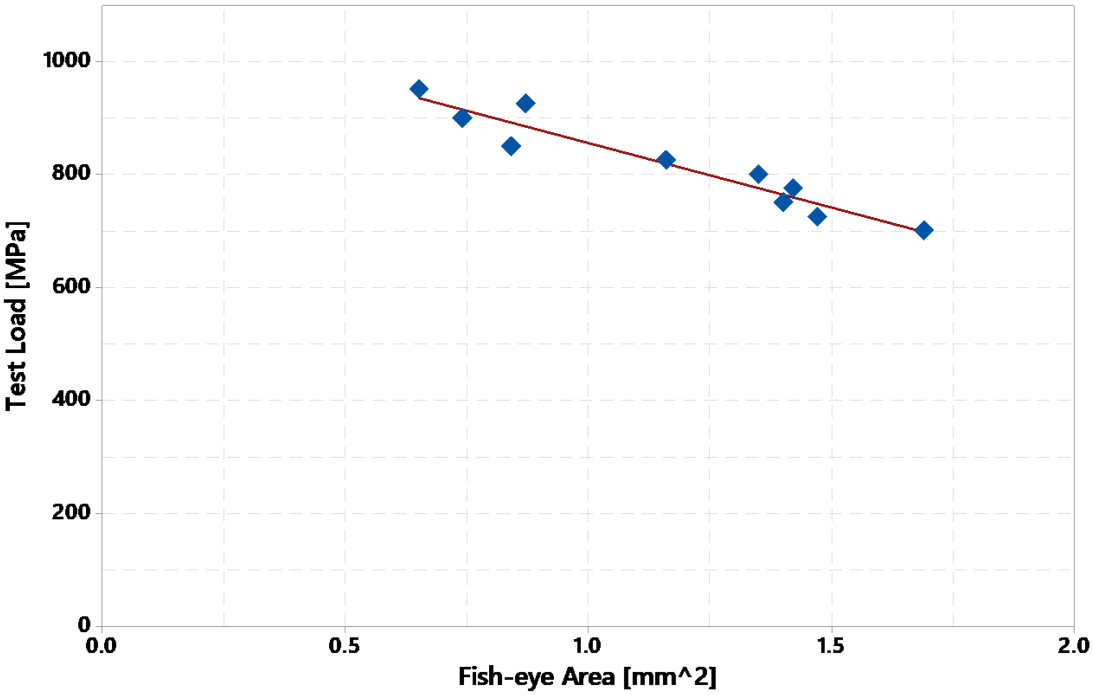

Figure 15. Scatter Plot of the correlation between fish-eye area and test load.

In particular, the correlation between the fish-eye area and the number of cycles seems to follow a nonlinear positive trend (Spearman Coefficient R = 0.806, p-Value < 0.01), and the relationship between the fish-eye area and the test load is a negative linear trend (Spearman Coefficient R = −0.952, p-Value < 0.01).

The subsurface crack initiation is probably caused by reaching the fatigue fracture limit of the bainitic matrix, which led to the formation of the facetted initiation planes, as confirmed by Figure 16. This feature is interesting because, although the level of nonmetallic

inclusions present in the material is higher than the hardened reference, this did not affect the outcome of the tests.

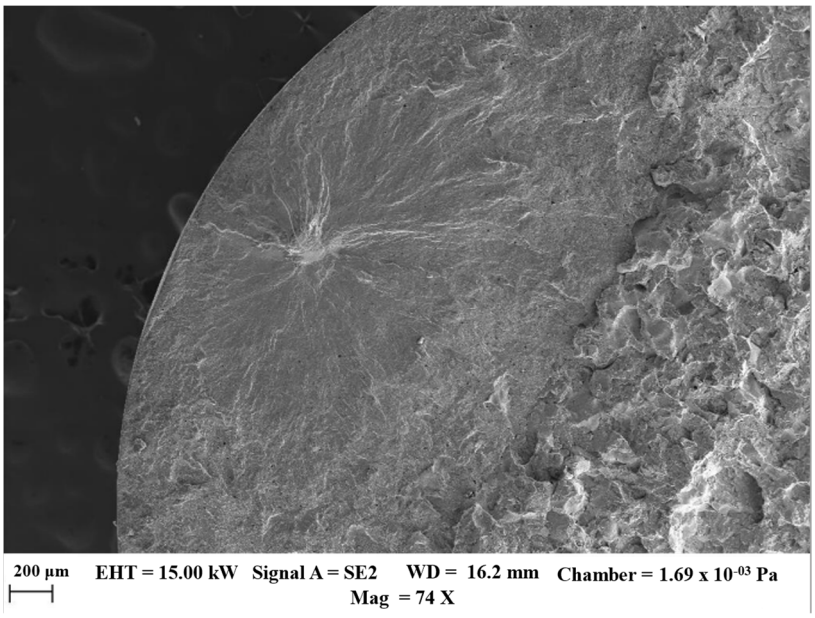

Figure 16. Crack initiation in the metallic matrix and limited fatigue propagation.

Lastly, the nitrided layer acts as a barrier for the crack initiation by moving it under the surface and as a limit for the propagation phase. In fact, fatigue does not progress in the nitrided layer, which breaks apart as soon as the fatigue limit is exceeded (Figure 17).

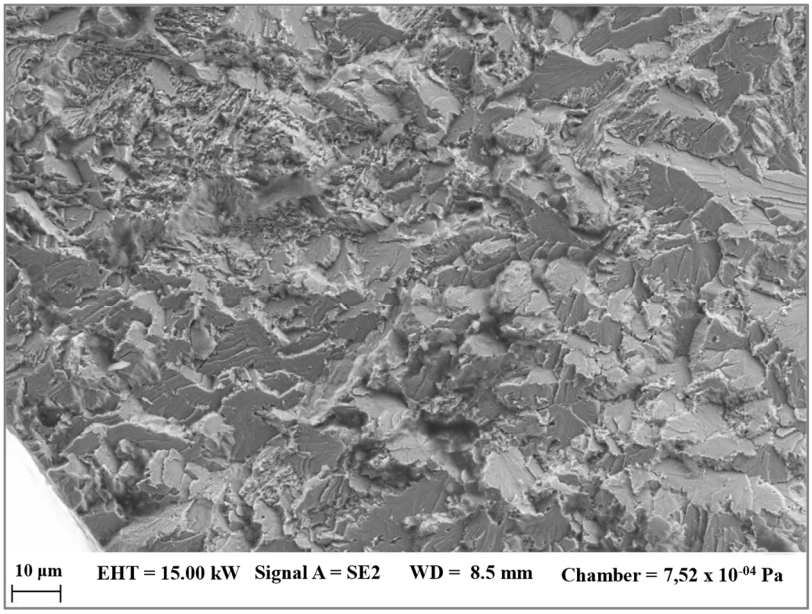

Figure 17. Morphology of the nitrided area near crack initiation.

3.4. Residual Stress Analysis

The residual stresses in the nitriding zone have been evaluated through several measurements taken at different depth levels (Figure 18). A comparison is also made between nitrided and untreated specimens' stresses on the external surfaces. In this case, the analysis has been made in longitudinal and transversal directions in the notched area of polished specimens (Figure 19).

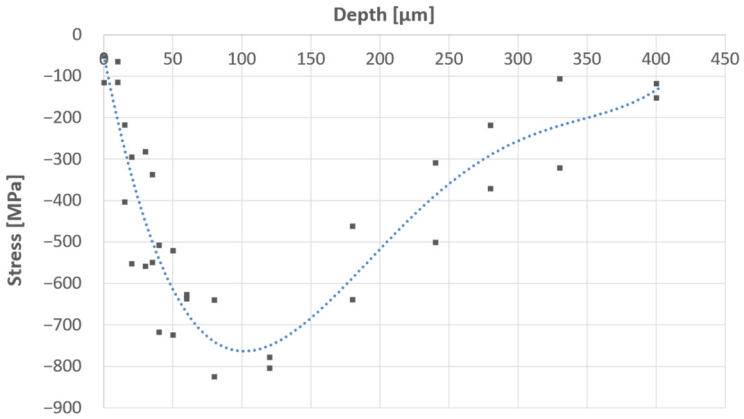

Figure 18. Residual stress in the nitriding zone at different depth levels.

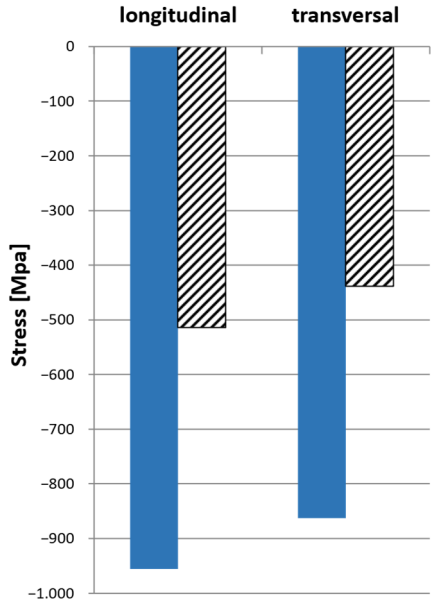

Figure 19. Comparison of residual stresses on external surface for nitride (blue bars) and not nitride (black hatched bars) specimen obtained by XRD.

Results confirm an increase in the residual stresses due to the nitriding diffusion process and machining operations. It is relevant to underline that the non-nitrided material on the external polished surface also shows a compression state. This is due to the heat treatment process (quench and temper) and machining operations performed after it (grinding and polishing). The main effect of compression residual stresses is clearly shown in rotating bending fatigue nitrided specimens where subsurface nucleations appear, while this phenomenon does not appear in non-nitrided specimens.

4. Conclusions

The steel analysed is a bainitic grade steel with high mechanical characteristics and high potential as an alternative material to quenched and tempered steels currently used for high-performance automotive engines, particularly in producing crankshafts. The research aims to characterise the steel's fatigue resistance considering nitriding's effect. The untreated material has excellent fatigue results considering its mechanical properties (>50% of Rm). Moreover, the fatigue crack propagates about 30% of the resistant section.

The nitriding applied to increase the fatigue property of the steel leads to good results in realising the nitrided layer, but the expected values of fatigue obtained are not so much improved. In fact, the fatigue limit increase compared to the untreated specimen is only 13% higher. The reason for such a low increase in fatigue limit could be found in the low ductile

behaviour of this steel, the high speed of stress application added, and the embrittlement of the nitriding treatment, as confirmed through fracture surface analysis.

Further investigations must be performed to increase the steel's ductile behaviour by using different heat treatments and going further in understanding the nucleation and propagation of cracks in bainitic materials using highly notched specimens to force the nucleation and propagation outside on the external surface.

Author Contributions: Conceptualisation, A.G. and U.M.; investigation, A.G. and U.M.; methodology, A.G. and U.M.; formal analysis, A.G. and U.M.; visualisation, A.G. and V.L.B.; data curation, A.G. and V.L.B.; writing—original draft, A.G. and U.M.; writing—review and editing, A.G., U.M. and V.L.B.; supervision, P.C. All authors have read and agreed to the published version of the manuscript.

Funding: This research received no external funding.

Institutional Review Board Statement: Not applicable.

Informed Consent Statement: Not applicable.

Data Availability Statement: Not applicable.

Conflicts of Interest: The authors declare no conflict of interest.

References

1. Cavallini, C.; Giorgetti, A.; Citti, P.; Nicolaie, F. Integral aided method for material selection based on quality function deployment and comprehensive VIKOR algorithm. *Mater. Des.* **2013**, *47*, 27–34. [CrossRef]
2. Giorgetti, A.; Cavallini, C.; Arcidiacono, G.; Citti, P. A mixed C-VIKOR fuzzy approach for material selection during design phase: A case study in valve seats for high performance engine. *Int. J. Appl. Eng. Res.* **2017**, *12*, 3117–3129.
3. Ceccanti, F.; Giorgetti, A.; Cavallini, C.; Arcidiacono, G.; Citti, P. Comparative evaluation of fuzzy axiomatic design and IAMS comprehensive VIKOR approaches for material selection in mechanical design. *Int. J. Eng. Res. Technol.* **2020**, *13*, 80–87. [CrossRef]
4. Giorgetti, A.; Girgenti, A.; Citti, P.; Delogu, M. A novel approach for axiomatic-based design for the environment. In *Axiomatic Design in Large Systems: Complex Products, Buildings and Manufacturing Systems*; Springer International Publishing: Berlin/Heidelberg, Germany, 2016; pp. 131–148.
5. Citti, P.; Giorgetti, A.; Millefanti, U. Current challenges in material choice for high-performance engine crankshaft. *Procedia Struct. Integr.* **2018**, *8*, 486–500. [CrossRef]
6. Sun, Y.; Bell, T. Plasma surface engineering of low alloy steel. *Mater. Sci. Eng. A* **1991**, *140*, 419–434. [CrossRef]
7. Genel, K.; Demirkol, M.; Capa, M. Effect of Ion Nitriding on Fatigue Behaviour of AISI 4140 Steel. *Mater. Sci. Eng.* **2000**, *279*, 208. [CrossRef]
8. Limodin, N.; Verreman, Y. Fatigue strength improvement of a 4140 steel by gas nitriding: Influence of notch severity. *Mat. Sci. Eng. A* **2006**, *435–436*, 460–467. [CrossRef]
9. Mei, J.; Xing, S.; Vasu, A.; Chunga, J.; Desai, R.; Dong, P. The fatigue limit prediction of notched components—A critical review and modified stress gradient based approach. *Int. J. Fatigue* **2020**, *135*, 105531. [CrossRef]
10. Hoja, S.; Steinbacher, M.; Zoch, H.-W. Compound Layer Design for Deep Nitrided Gearings. *Metals* **2020**, *10*, 455. [CrossRef]
11. Citti, P.; Giorgetti, A.; Millefanti, U. Citti, Paolo; Mechanical characterisation of a new low carbon bainitic steel for high performance crankshaft. *Procedia Struct. Integr.* **2018**, *12*, 438–447. [CrossRef]
12. Dixon, J.; Mood, A.M. A method for obtaining and analysing sensitivity data. *J. Am. Stat. Assoc.* **1948**, *43*, 109–126. [CrossRef]
13. Sunkwang, K.; Sungook, Y.; Jun-Ho, K.; Soon, P. The Effect of the Transformation of ε-Fe2-3N into γ′-Fe4N phase on the Fatigue Strength of Gas-Nitrided Pure Iron. *Metals* **2020**, *10*, 823. [CrossRef]
14. Jasinski, J.J.; Kurpaska, L.; Fraczek, T.; Lubas, M.; Sitarz, M. Structural Characterization of Fine γ′-Fe_4N Nitrides Formed by Active Screen Plasma Nitriding. *Metals* **2020**, *10*, 1656. [CrossRef]
15. Bell, T.; Loh, N. The fatigue Characteristics of Plasma Nitrided Three Pct. Cr-Mo Steel. *J. Heat Treat.* **1982**, *2*, 232–237. [CrossRef]
16. Yakura, R.; Matsuda, M.; Sakai, T.; Ueno, A. Effect of Inclusion Size on Fatigue Properties in Very High Cycle Region of Low Alloy Steel Used for Solid type Crankshaft. *R. D Res. Dev. Kobe Steel Eng. Rep.* **2016**, *1*, 20–24.
17. Zhou, C.; Wanga, M.; Hui, W.; Dong, H.; Wang, L.; Wu, R. Rotating bending fatigue properties of two case hardening steels after nitriding treatment. *Mater. Des.* **2013**, *46*, 539–545. [CrossRef]
18. Forrest, P.G. *Fatigue of Metals*; Pergamon: Oxford, UK, 1968.
19. Terent'ev, V.F.; Michugina, M.S.; Kolmakov, A.G.; Kvedaras, V.; Čiuplys, V.; Čiuplys, A.; Vilys, J. The effect of nitriding on fatigue strength of structural alloys. *Mechanika* **2007**, *64*, 12–22.
20. Hernández-Rengifo, E.; Rodríguez, S.A.; Coronado, J.J. Improving fatigue strength of hydromachinery 13Cr-4Ni CA6NM steel with nitriding and thermal spraying surface treatments. *Fatigue Fract. Eng. Mater. Struct.* **2021**, *44*, 1059–1072. [CrossRef]

21. Gui, X.; Gao, G.; An, B.; Misra, R.D.K.; Bai, B. Relationship between non-inclusion induced crack initiation and microstructure on fatigue behavior of bainite/martensite steel in high cycle fatigue/very high cycle (HCF/VHCF) regime. *Mater. Sci. Eng. A* **2021**, *803*, 140692. [CrossRef]
22. Huang, Z.; Wagner, D.; Bathias, C.; Paris, P.C. Subsurface crack initiation and propagation mechanisms in gigacycle fatigue. *Acta Mater.* **2010**, *58*, 6046–6054. [CrossRef]
23. Murakami, Y. The mechanism of fatigue failure in the very high cycle fatigue (VHCF) life regime of N > 10^7 cycles. In *Metal Fatigue: Effects of Small Defects and Non-Metallic Inclusions*; Elsevier: Amsterdam, The Netherlands, 2002.
24. Sakai, T. Review and prospects for current studies on very high cycle fatigue of metallic materials for machine structural use. *J. Solid Mech. Mat. Eng.* **2009**, *3*, 425–439. [CrossRef]
25. Shiozawa, K.; Morii, Y.; Nishino, S.; Lu, L. Subsurface crack initiation and propagation mechanism in high strength steel in a very high cycle fatigue regime. *Int. J. Fatigue* **2006**, *28*, 1521–1532. [CrossRef]
26. Zhang, J.W.; Lu, L.T.; Shiozawa, K.; Zhou, W.N.; Zhang, W.H. Effect of nitrocarburising and post-oxidation on fatigue behavior of 35CrMo alloy steel in very high cycle fatigue regime. *Int. J. Fatigue* **2011**, *33*, 880–886. [CrossRef]
27. Murakami, Y.; Endo, M. Effects of defects, inclusions and inhomogeneities on fatigue strength. *Int. J. Fatigue* **1994**, *16*, 163–182. [CrossRef]